Enhanced bandwidth of supercontinuum generated in microstructured fibers

G. Genty, M. Lehtonen, and H. Ludvigsen

Fiber-Optics Group, Department of Electrical and Communications Engineering, Helsinki University of Technology, P.O. Box 3500, FIN-02015 HUT, Finland
goery.genty@hut.fi

M. Kaivola

Department of Engineering Physics and Mathematics, Helsinki University of Technology, P.O. Box 2200, FIN-02015 HUT, Finland

Abstract: Enhancement of the bandwidth of supercontinuum generated in microstructured fibers with a tailored dispersion profile is demonstrated experimentally. The fibers are designed to have two zero-dispersion wavelengths separated by more than 700 nm, which results in an amplification of two dispersive waves at visible and infrared wavelengths. The underlying physics behind the broad continuum formation is discussed and analyzed in detail. The experimental observations are confirmed through numerical simulations.

OCIS codes: (190.5530) Pulse propagation and solitons; (230.3990) Microstructure devices;

References and links

1. J. K. Ranka, R. S. Windeler, and A. J. Stentz, "Visible continuum generation in air-silica microstructure optical fibers with anomalous dispersion at 800 nm," Opt. Lett. **25**, 25-27 (2000).
2. See for example *Nonlinear optics of photonic crystals*, Special issue of J. Opt. Soc. Am. B **19**, 1961-2296 (2002) or *Supercontinuum generation*, Special issue of Appl. Phys. B **77**, 143-376 (2003).
3. A. V. Husakou and J. Herrmann, "Supercontinuum generation in photonic crystal fibers made from highly nonlinear glasses, " Appl. Phys. B. **77**, 227-234 (2003).
4. K. M. Hilligsøe, T. V. Andersen, H. N. Paulsen, C. K. Nielsen, K. Mølmer, S. Keiding, R. Kristiansen, K. P. Hansen, and J. J. Larsen, "Supercontinuum generation in a photonic crystal fiber with two zero dispersion wavelengths, " Opt. Express **12,** 1045-1054 (2004), http://www.opticsexpress.org/abstract.cfm?URI=OPEX-12-6-1045
5. R. Holzwarth, T. Udem, T. W. Hansch, J. C. Knight, W. J. Wadsworth, and P. S. J. Russell, "Optical frequency synthesizer for precision spectroscopy," Phys. Rev. Lett. **85**, 2264-2267 (2000).
6. A. V. Husakou and J. Herrmann, "Supercontinuum generation, four-wave mixing, and fission of higher-order solitons in photonic-crystal fibers," J. Opt. Soc. Am. B **19**, 2171-2182 (2002).
7. G. Genty, M. Lehtonen, H. Ludvigsen, J. Broeng, and M. Kaivola, "Spectral broadening of femtosecond pulses into continuum radiation in microstructured fibers," Opt. Express **10**, 1083-1098 (2002), http://www.opticsexpress.org/abstract.cfm?URI=OPEX-10-20-1083
8. J. M. Dudley, L. Provino, N. Grossard, H. Maillotte, R. S. Windeler, B. J. Eggleton, and S. Coen, "Supercontinuum generation in air-silica microstructured fibers with nanosecond and femtosecond pulse pumping," J. Opt. Soc. Am. B. **19**, 765-771 (2002).
9. J. R. Folkenberg, N. A. Mortensen, K. P. Hansen, T. P. Hansen, H. R. Simonsen, and C. Jakobsen, "Experimental investigation of cutoff phenomena in nonlinear photonic crystal fibers," Opt. Lett. **28**, 1882-1884 (2003).
10. N. Akhemediev and M. Karlsson, "Cherenkov radiation emitted by solitons in optical fibers," Phys. Rev. A **51**, 2602-2607 (1995).
11. K. J. Blow and D. Wood, "Theoretical description of transient stimulated Raman scattering in optical fibers," IEEE J. Quantum Electron. **25**, 2665-2673 (1989).

12. D. V. Skryabin, F. Luan, J. C. Knight, and P. St. J. Russell, "Soliton self-frequency shift cancellation in photonic crystal fibers," Science **301**, 1705-1708 (2003).
13. M. Lehtonen, G. Genty, M. Kaivola, and H. Ludvigsen, "Supercontinuum generation in a highly birefringent microstructured fiber," Appl. Phys. Let. **82**, 2197-2199 (2003).
14. M. L. Hu, C. Y. Wang, L. Chai, and A. M. Zheltikov, "Frequency-tunable anti-Stokes line emission by eigenmodes of a birefringent microstructure fiber," Opt. Express **12**, 1932-1937 (2004), http://www.opticsexpress.org/abstract.cfm?URI=OPEX-12-9-1932

1. Introduction

Microstructured fibers (MFs) possess unique optical properties which allow, e.g., generating supercontinua (SC) with a broader bandwidth than what is possible in bulk silica or in standard optical fibers. Since the first report on SC generation in a MF in 1999 [1], comprehensive efforts have been made to understand the physical mechanisms leading to the generation of light with a broad spectrum in this type of fiber, and an extensive literature has been published on the subject [2]. However, the possibility of tailoring the properties of MFs for improving the efficiency of SC generation with femtosecond pulses has been little explored. It was suggested in Ref. 3 that the use of a MF with two zero-dispersion points should result in a broader SC. We demonstrate experimentally this to be true for properly designed MFs with two zero-dispersion wavelengths located widely apart in the visible and infrared regions. We note that SC generation in a MF with two zero-dispersion wavelengths was recently demonstrated [4]. However, in this case, the zero-dispersion wavelengths were only separated by 160 nm and the SC was shown to result from the combined action of self-phase modulation and four-wave mixing. This mechanism limited the bandwidth of the SC to ~600 nm with a high input peak power in excess of 15 kW. Our experimental results greatly differ from Ref. 4. In particular, we see that the expansion of the continuum towards the infrared results from the continuous amplification of dispersive waves beyond the infrared zero-dispersion wavelength. Furthermore, we observe that the process of soliton self-frequency shift (SSFS) plays a crucial role as it permits to keep the pump wavelength close to the visible to efficiently generate blue wavelength components thus yielding an ultra-broad SC whose bandwidth extends from 390 nm to 1800 nm. Due to the SSFS and the negative slope of the dispersion curve at the infrared wavelengths, the dynamics of the infrared dispersive waves differs from the behavior of the corresponding waves at the visible wavelengths. The experimental observations are fully explained by numerical simulations.

2. Experiments

Coherent octave spanning SC can be generated in MFs by launching into the fiber femtosecond pulses with a wavelength located near the zero-dispersion wavelength (λ_{ZD}) of the MF [5]. For a pump wavelength on the anomalous side of λ_{ZD}, it has been shown that the fundamental mechanism leading to the SC generation mainly involves two distinct physical effects: Amplification of dispersive waves matched in phase with the pump extends the SC to the blue [3,6,10], whereas pulse splitting and multiple SSFSs are responsible for the spreading of the SC into the infrared [7,8].

The bandwidths of the continua reported in the literature typically do not extend below 380 nm for the fundamental mode. The short cut-off wavelength of MFs can be located well below 400 nm [9] and, consequently, it should not be a factor limiting the extension of SC towards shorter wavelengths. Rather, the main limiting factor is usually due to the relative location of the λ_{ZD} with respect to the pump wavelength. The further the pump wavelength is tuned from λ_{ZD} in the anomalous dispersion region, the deeper in the blue the short wavelength components are generated. However, this occurs at the expense of increasing of the width of the gap between the pump and the blue wavelength components, and also, for the case of large detuning between the pump and λ_{ZD}, the amplitude of the blue components will drastically reduce. For this reason, the pump wavelength should not be tuned too far away from the λ_{ZD} in order to allow for a reasonable optical signal at the blue wavelengths to be

obtained [7]. As a consequence, this may then limit the extension of the continuum towards the infrared.

   To increase the bandwidth of the SC into the infrared, one can take advantage of the same physical mechanism that is responsible for the generation of the blue wavelength components, as is illustrated in Fig. 1. A pump wave whose spectrum partially extends into the normal dispersion region of the MF will amplify dispersive waves at wavelengths located beyond λ_{ZD}. Therefore, designing a MF so that it has two λ_{ZD}'s, one in the visible (λ_{ZDV}) and another in the vicinity of 1500 nm (λ_{ZDI}), should allow for the generation of spectral components further into the infrared. Indeed, if under the action of SSFS the center wavelengths of the multiple solitons that are split from the initial pump pulse shift into the vicinity of λ_{ZDI}, these solitons can act as pumps for the amplification of dispersive waves beyond λ_{ZDI}. In this way, a substantial increase of the bandwidth of the SC in the infrared can be obtained while still efficiently generating the blue wavelength components.
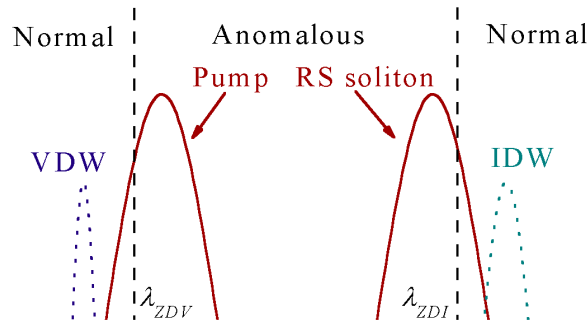
Fig. 1. Schematic of the spectral amplification of dispersive waves along a two-λ_{ZD} MF. VDW: visible dispersive wave, IDW: infrared dispersive wave, RS soliton: Raman shited soliton.

   Enhancement of the supercontinuum bandwidth in a two-λ_{ZD} MF is here experimentally demonstrated in four fused silica MFs that exhibit different dispersion properties. The continua were pumped by 200 fs pulses from a Ti:Sapphire laser (Spectra Physics/Tsunami). The characteristic properties of the fibers are summarized in Table 1 and their dispersion profiles are plotted as functions of wavelength in Fig. 2(a). The calculated variation of the effective area with wavelength for the four fibers is presented in Fig. 2(b).

Table 1. Characteristic properties of the MFs. Λ: pitch, d: hole diameter, and MFD: mode-field diameter.

	Fiber 1	Fiber 2	Fiber 3	Fiber 4
Λ (µm)	1.4	1.37	1.33	1.22
d/Λ	0.67	0.65	0.62	0.63
MFD (µm) @ 800 nm	1.3	1.3	1.2	1.1
Visible λ_{ZD} (nm)	740	730	750	690
Infrared λ_{ZD} (nm)	1700	1610	1515	1390
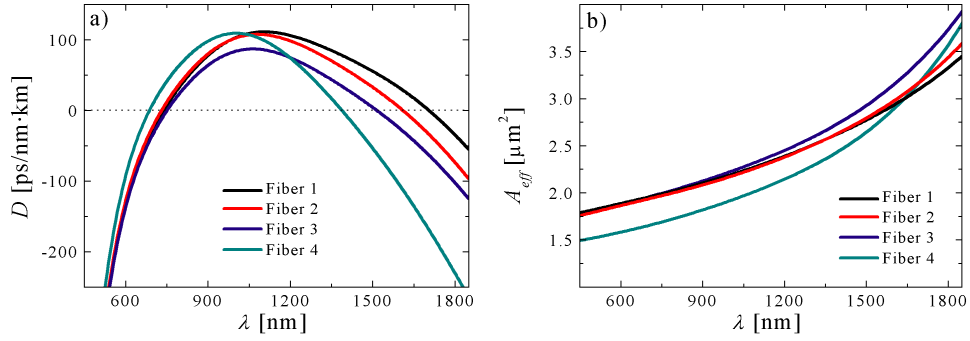
Fig. 2. Calculated dispersion profile a) and effective area b) of the four MFs. D: dispersion and A_{eff}: effective area.

The spectra of the continua generated along 1.5 m of the MFs for different input powers are displayed in Fig. 3. The visible part of the continuum is similar for the four fibers. This is readily explained by the fact that all the fibers exhibit comparable dispersion profiles at the shorter wavelengths. For a low input power, the SC spectra do not extend into the range of λ_{ZDI} and no spectral components beyond λ_{ZDI} are observed. However, as the input power is increased, the SC expands closer to λ_{ZDI}, and as the spectrum reaches this point, a broad peak beyond λ_{ZDI} also appears in the case of the fibers 2-4. For similar input power values, the center wavelength and magnitude of this peak decreases and increases, respectively, from fiber 2 to fiber 3 to fiber 4.
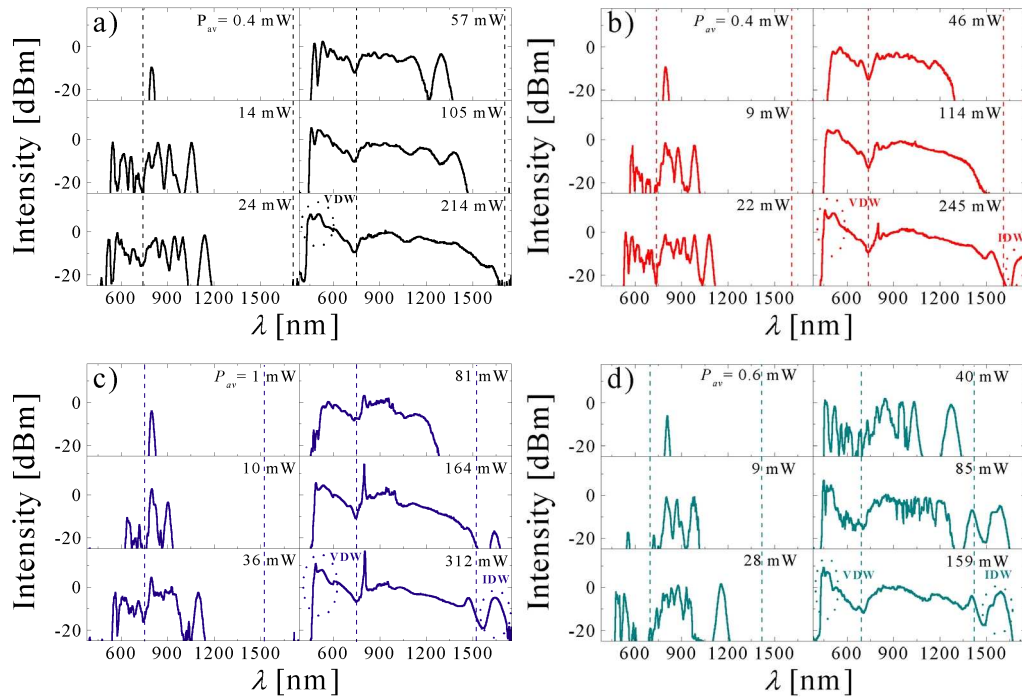
Fig. 3. Experimental spectra for increasing input power recorded at the output of a) fiber 1, b) fiber 2, c) fiber 3, and d) fiber 4. The dashed lines shows the location of λ_{ZD}. P_{av}: average pump input power, VDW: visible dispersive wave, and IDW: infrared dispersive wave. The length of the fibers is 1.5 m, λ_P=800nm, and $\Delta\tau$=200 fs. The measurement range of the spectrum extends from 350 to 1750 nm. The drop of the spectral intensity at longer wavelengths is partly due to the decreasing sensitivity of the spectrum analyzer.

Provided a large spectral overlap exists, energy from the pump located in the anomalous dispersion region of the MF is efficiently transferred to dispersive waves which are phase-matched with the pump [3,6]. The center frequencies of these waves fall in the normal dispersion region of the MF and are determined by the phase-matching condition

$$\Delta\beta = \beta(\omega_P) - \beta(\omega_{DW}) = (1 - f_R)\gamma(\omega_P)P_P - \sum_{n\geq 2}\frac{(\omega_{DW} - \omega_P)^n}{n!}\beta_n(\omega_p) = 0 , \qquad (1)$$

where $\beta(\omega_P)$ and $\beta(\omega_{DW})$ represent the propagation constants at the angular frequency of the pump ω_P and the dispersive wave ω_{DW}, respectively. Here, γ is the nonlinear coefficient of the MF and $\beta_n(\omega_P)$ denotes the nth term in the Taylor-series expansion of β around ω_P. The factor f_R accounts for the fractional contribution of the Raman delayed response of the fiber and P_P is the peak power of the pump. For any pump wavelength located in the anomalous dispersion region of the fiber, the number of solutions to Eq. (1) equals the number of zero-dispersion wavelengths of the fiber. Figure 4 illustrates the calculated center wavelengths for the dispersive waves λ_{DW} as a function of the pump wavelength λ_P for the four MFs used in the experiments. The contribution of the nonlinear phase-shift is neglected.
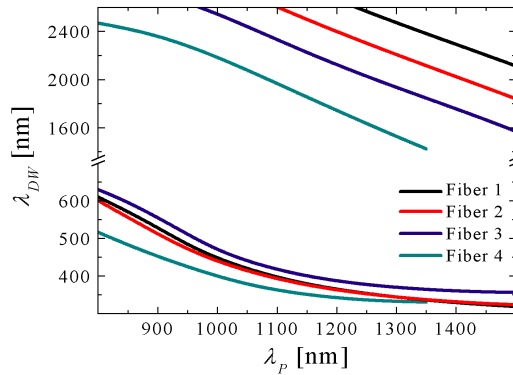
Fig. 4. Calculated center wavelength of the dispersive waves as a function of the pump wavelength for the four MFs. The black, red, blue, and green curves correspond to fiber 1, 2, 3, and 4, respectively.

Due to the existence of two λ_{ZD}'s in the fibers there are two solutions for the center wavelength of the dispersive waves; one in the visible and another one in the infrared normal dispersion region. The center wavelength of the dispersive wave in the visible behaves very similarly for the fibers 1-3 as could be expected from Fig. 2(a). The wavelength is slightly shorter for fiber 4, since λ_{ZDV} is located at a shorter wavelength for this fiber. These predictions are in reasonable agreement with the experimental SC spectra of Fig. 3. The situation is different for the infrared dispersive waves, as the dispersion profiles of the four fibers substantially differ at the infrared wavelengths. In particular, for a given pump wavelength, the closer the λ_{ZDI} of the MF is to the pump wavelength, the closer to the pump the infrared dispersive wave is located in the spectrum. This is also in agreement with the experiments. Note that the dispersive wave is effectively amplified only if the overlap between the spectrum of the pump and that of the dispersive wave is large enough. In practice, this means that the wavelength of the pump should be close to λ_{ZDV}.

The onset of the continuum formation can now be explained as follows. The wavelength of the pump pulse is initially close to λ_{ZDV}, which results in a strong amplification of the blue dispersive waves. Under the action of Raman scattering, the pump pulse splits into multiple solitons that subsequently experience soliton self-frequency shift. As the center wavelengths of the soltions shift closer to λ_{ZDI}, amplification of the infrared dispersive waves can take place, resulting in a broad peak in the spectrum located beyond λ_{ZDI}. The amplification of the

infrared dispersive waves depends on their spectral overlap with the solitons having their center wavelengths in the vicinity of λ_{ZDI}. The overlap increases as the solitons shift closer to λ_{ZDI} and, consequently, the infrared dispersive waves becomes clearly visible in the experimental spectrum when the center wavelengths of the solitons are located less than ~100 nm away from λ_{ZDI}. It can be seen from Fig. 4 that the infrared dispersive wave should then be located at around 2000, 1800, 1600 and 1550 nm for the MFs 1-4, respectively. This is backed up by the spectra presented in Fig. 3.

3. Simulations

To confirm the experimental observations, the propagation of femtosecond pulses along fiber 4 was simulated by solving numerically the nonlinear Schrödinger equation with a standard split-step Fourier algorithm [11]. The propagation modeling includes the full propagation constant of the MF, the Raman delayed response of the fiber, and the self-steepening effect. The wavelength dependence of the losses and of the effective area of the fiber were also included in the model. The simulated spectrum at the output of 1 m of fiber 4 plotted in Fig. 5 is in qualitative agreement with the experiments (see Fig. 3(d), last spectrum). In particular, the location of the visible and infrared dispersive waves is well reproduced taking into account the experimental uncertainties in the exact input power, pulse width and dispersion of the MF.
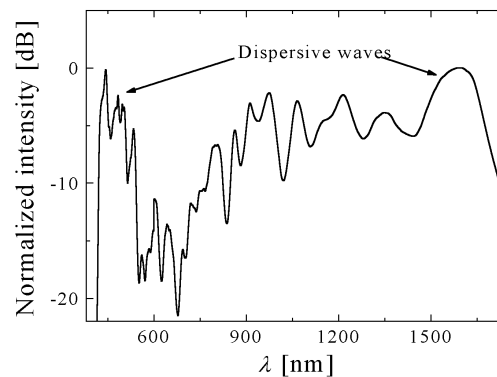
Fig. 5. Simulated spectrum of the SC generated along 1 m of fiber 4. P_{av}=140 mW, $\Delta\tau$=200 fs, and λ_P=800 nm. For better comparison, the simulated spectrum was averaged over the same spectral window as is the resolution bandwidth of the optical spectrum analyzer applied in the experiments.

Physical insight can be gained by plotting the simulated spectrogram of the pulse for different propagation lengths z along the MF, as is illustrated in Fig. 6. Under the combined action of self-phase modulation and dispersion, the pulse compresses in the first centimeter of the MF, which results in a spectral broadening of the pulse (see Fig. 6(a)). As the spectrum of the pulse overlaps with that of the visible dispersive wave, the latter one is strongly amplified (see Fig. 6(b)). The pulse splits into multiple solitons that subsequently experience SSFS (see Fig 6(b)-(d)). When the center wavelengths of the solitons shift into the vicinity of λ_{ZDI}, infrared dispersive waves start to be amplified (see Fig. 6(c)-(d)) and, as in the case of the formation of the visible dispersive waves, a gap is formed around λ_{ZDI}. Furthermore, it can be seen from Fig. 6(d) that the infrared dispersive waves spread quickly in time. This confirms their dispersive nature. Even though the physical origin of the dispersive waves at the visible and infrared wavelengths is identical, their subsequent evolution is drastically different. Indeed, the slope of the dispersion curve around the visible zero-dispersion wavelength is positive whereas that around the infrared zero-dispersion wavelength is negative. Consequently, the spectra of the multiple solitons are moving away from the spectral components of the visible dispersive waves towards the infrared. This fundamental difference

explains the fact that the visible dispersive waves are generated in the very beginning of the MF and are not subsequently affected by further propagation whereas the infrared dispersive waves are amplified along the way and their spectrum broadens as the solitons shift their wavelength closer to λ_{ZDI}. This results in a reduced gap at λ_{ZDI} compared to the one on the visible side. The solitons eventually cease to shift their center wavelength as they transfer energy into the infrared waves. The recoil due to this energy loss downshifts the center wavelength of the solitons and balances the Raman upshift [12]. We also want to point out that the interaction between the multiple solitons and the infrared dispersive waves results in a strong modulation of the dispersive waves (see Fig. 6(d)).
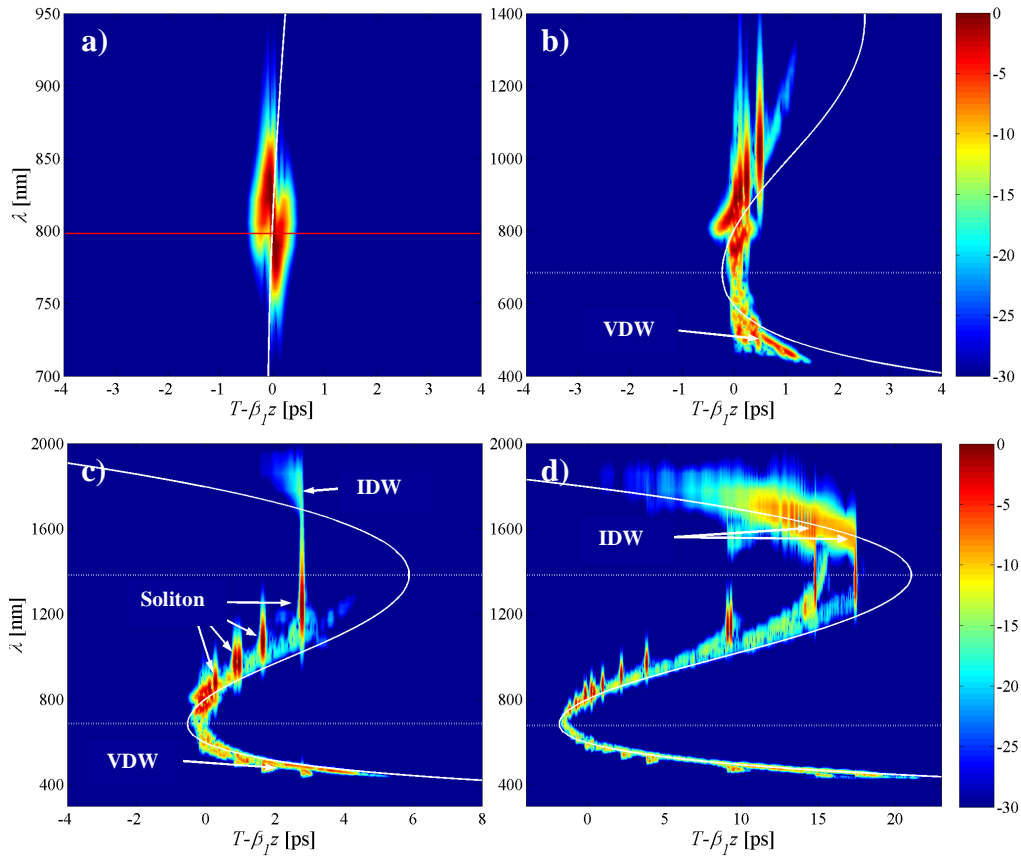
Fig. 6. Simulated spectrogram after propagation in fiber 4 for a) z=1 cm, b) z=6 cm, c) z=14 cm and d) z=50 cm. P_{av}=60 mW, λ_P=800 nm, and $\Delta\tau$=200 fs. The red line marks the pump wavelength and the dotted lines represent the λ_{ZD}'s. The white curve corresponds to the group delay of the fiber. VDW: visible dispersive wave and IRW: infrared dispersive wave.

The sequence of events described above can conveniently be visualized in the movie of Fig. 7. For clarity, the scale of the x-axis changes as the pulse propagates into the MF. The propagation length is displayed in the top left corner of the frame and the dotted white lines mark the zero-dispersion wavelengths of the MF.
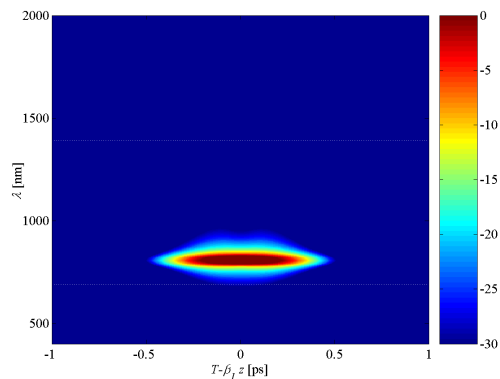
Fig. 7. (Movie 2.8 MB) Simulated evolution of the spectrogram of the pulses along fiber 4. The pump pulse parameters are the same as those in Fig. 6.

4. Discussion

We also analyzed the effects of changing the pump wavelength and varying the width of the input pulses on the resulting continuum. Various SC spectra recorded for different pump wavelengths and input pulse widths are presented in Figs. 8(a) and 8(b) for pulses propagating along 1.5 m of fiber 4.

In practice, it is very difficult to control the input power and/or the width of the input pulses while tuning the pump wavelength. Nevertheless, experiments shows that for high values of input power (in our case greater than ~100 mW), a small variation in input power does not affect the overall spectral shape of the SC. The effect of detuning the pump wavelength on the generated SC can be seen by comparing the second spectra of Fig. 8(a) and Fig. 8(b), and the last spectrum of Fig. 8(a) with the first spectrum of Fig. 8(b) as the pulse width and input power are more or less similar for these two pairs. In particular, varying the pump wavelength in the anomalous dispersion region does not substantially affect the bandwidth of the continuum. The spectrum of the SC extends slightly more into the blue for a longer pump wavelength in agreement with Fig. 4. At the same time, the width of the gap at λ_{ZDV} is increased [7,13]. The drastic reduction of the bandwidth of the SC on the infrared side observed in the top spectrum of Fig. 8(a) is due to the low average power coupled into the MF in this case. Due to a substantial variation of the dispersion as the pump wavelength is increased, the detuning of the pump has a stronger impact on the smoothness of the continuum compared to the input pulse width as discussed in Ref. 13.

It can also be seen that the width of the pump pulses has a rather minor influence on the bandwidth of the SC for the range of values investigated. In particular, even though the input power slightly varies the spectral width of the infrared dispersive wave component is nearly unchanged. The increase of the width of the infrared peak observed in the bottom spectrum of Fig. 8(b) compared to the two fist spectra of the same figure is attributed to the higher energy of the pump pulse. Again, the most noticeable effect of the pulse width is on the flatness of the SC, the flatter SC spectra being obtained by launching broader pulses at shorter pump wavelengths in agreement with previously reported results [13]. It is also expected that the use of much shorter pulses on the order of 50 fs will result in a degradation of the smoothness of the SC.

Figure 8(c) shows the spectrum of a SC recorded experimentally at the output of 50 cm of fiber. The spectrum is very similar to the one recorded for a fiber length of 1.5 m (see Fig. 3(d)), which indicates that the generation of the continuum is already complete at 50 cm of propagation for an input power of ~150 mW. This fact is also confirmed by the simulations (see Fig. 7).
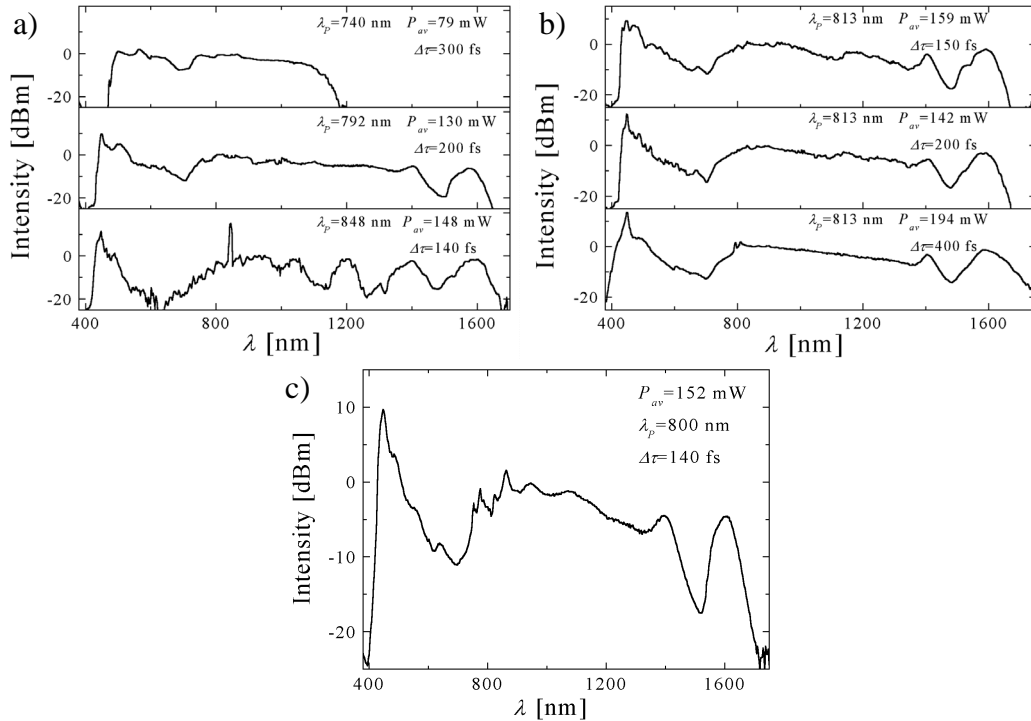
Fig. 8. Supercontinuum spectrum recorded when a) tuning the pump wavelength and b) varying the input pulse. c) Supercontinuum generated in 50 cm of fiber 4.

Beyond 1700 nm, the wavelength exceeds by far the size of the core of the MFs used in the experiments, which affects the guiding properties and results in high leakage losses. In the case of fiber 4, the simulations predict that the bandwidth of the SC can extend close to 2000 nm if the leakage losses beyond 1700 nm could be reduced. This could possibly be achieved by increasing the core size. The hole diameter should also be varied accordingly in order to retain the same dispersion profile. Also, the use of highly-birefringent MFs would provide a convenient way to tune the properties of the SC at the infrared wavelengths similarly to what was previously demonstrated for the blue wavelength components [13,14].

Introducing a zero-dispersion wavelength in the infrared clearly offers advantages for supercontinuum generation with femtosecond pulses. In the general case, amplification of the dispersive waves is a more efficient mechanism for transferring energy to the longer wavelengths than SSFS. In particular, as dispersion increases, the width of a soliton pulse increases as well and the overlap between the soliton spectrum and that of the Raman gain reduces, which, in turn, decreases the rate of the wavelength shift. Also, SSFS requires much longer length of fiber to transfer the energy to the longer wavelengths than is the case with the amplification of the dispersive waves.

The optimum location of the second zero-dispersion wavelength is essentially influenced by the requirement that the soliton spectrum must extend into the λ_{ZDI} range. How far λ_{ZDI} can be pushed mainly depends on three factors: input pulse energy, strength of the fiber nonlinearity and leakage losses of the MF at the infrared wavelengths. In particular, the further the infrared zero-dispersion is located from the pump wavelength, the more input power is required to shift the multiple solitons into the vicinity of λ_{ZDI}. Also, shifting λ_{ZDI} further into the infrared implies a MF with larger core and reduced strength of the nonlinearity. Then again, higher input power or longer fiber length is required. Finally, the infrared zero-dispersion wavelength must be located in a range where the leakage losses are not too high so that amplification of the dispersive waves beyond this wavelength is possible.

5. Conclusion

We have through experiments and simulations investigated the gain brought about by tailored dispersion profiles of MFs for enhanced supercontinuum generation. We could demonstrate that the introduction of a second zero-dispersion wavelength in the infrared allows extending the spectrum of the SC in the fundamental mode up to 1800 nm. The enhancement of the bandwidth was shown to result from the amplification of the dispersive waves in the normal dispersion region of the MF. In this way, a broad, relatively flat continuum spanning from 390 to 1800nm was successfully generated. The design and analysis presented here opens up the possibility of generating even broader continua in pure silica microstructured fibers by properly tailoring the dispersion profile.

Acknowledgments